International Journal of Hydrogen Energy 49 (2024) 1176–1191

Contents lists available at ScienceDirect

International Journal of Hydrogen Energy

journal homepage: www.elsevier.com/locate/he

Effects of hydrogen enrichment on the heat generation and emission of natural gas turbulent premixed flame

Abdulhadi Odeh, Manosh C. Paul *

Systems, Power & Energy Research Division, James Watt School of Engineering, University of Glasgow, Glasgow, G12 8QQ, United Kingdom

ARTICLE INFO

Keywords:
Hydrogen enrichment
Natural gas
Turbulent premixed flame
Domestic boiler
Combustion modelling

ABSTRACT

The demand for clean energy and the decarbonisation targets set globally require researching and developing new solutions. An efficient computational approach was implemented to examine the effect of hydrogen enrichment on flame characteristics, flame temperature, heat generation, NO_x and carbon emissions under varying stoichiometry of combustion. Results showed that hydrogen enrichment significantly reduces CO_2 emissions but also has undesirable effects which include reducing the heat generation capability of flame and increasing NO_x emissions. The level of impact on each of these characteristics was found to be different. Under a boiler-like condition and stoichiometry ($\Phi = 0.8$), a 10 % decrease in CO_2 emissions was observed when enriching the fuel with 20 % hydrogen. Concurrently, the heat flux generated from the flame is reduced by 6 % and NO_x emission is increased by 2 %. The effect of hydrogen enrichment on these aspects becomes more prominent at a higher enrichment level. The study also finds that making combustion leaner is an effective strategy to combat the effect of hydrogen enrichment with respect to CO_2 and NO_x emission generation. Despite the leaner combustion producing less emissions for any given hydrogen enrichment level, it significantly decreases the heat transfer capacity of the flame. Alongside these flame characteristics, the significant role of hydrogen enrichment on increasing water vapour (H_2O) production was examined.

1. Introduction

Decarbonisation is becoming increasingly important to tackle climate change. There are several routes for decarbonisation in the domestic heating sector. Among the promising solutions that can potentially be adopted is blending hydrogen (H_2) with natural gas which is primarily comprised of methane (CH_4).

An analytical study conducted by Shiro et al. [1] reveals that hydrogen blending significantly decreases carbon dioxide (CO_2) emissions. The study keeps both the thermal load and equivalence ratio fixed for fair comparison while varying the hydrogen volume fraction in the fuel. The study underlines the importance of water vapour production as one of the main challenges that face H_2/CH_4 blends. It reports that hydrogen enrichment results in higher H_2O production which implies that the heat exchanger will need to be re-assessed because high levels of H_2O result in lower efficiency. In addition, the ducts which discharge condensate in natural gas boilers might be undersized for hydrogen enriched fuels and will need to be redesigned [1].

Hydrogen (H_2) has a significantly wider flammability range, lower ignition energy and significantly higher burning velocity compared to methane [1]. The effects of hydrogen blending on flashback and blow off limits were assessed using empirical equations [1,2]. Numerical and experimental studies were also performed to assess the effect of hydrogen enrichment on the flame front structure and burning velocities of turbulent premixed flames [3,4]. Meanwhile, other studies 5–9 focused on understanding the preferential transport effects under varying hydrogen present in the fuel to highlight the effect of Lewis number on the accuracy of numerical modelling involving turbulent H_2/CH_4 premixed flames. An effective Lewis number approach was proposed by several studies which consider turbulent premixed combustion [7,8]. The proposed approach will be adopted in this study to consider the effect of preferential diffusion.

The effect of hydrogen enrichment on the emission generation of natural gas was experimentally investigated by Boulahlib et al. [10] in the context of staged combustion. The study concluded that NO_x decreases with the addition of H_2 beyond 20 vol%. This is a promising finding since it suggests that when using staged combustion, NOx will ultimately decrease with high concentrations of H_2 being present in the gas fuel. This finding is in the same direction as the study conducted by Pignatelli et al. [11] which concludes that adding hydrogen to methane fuel will result in a significantly lower NO_x level despite higher flame

* *Corresponding author.*
E-mail address: Manosh.Paul@glasgow.ac.uk (M.C. Paul).

https://doi.org/10.1016/j.ijhydene.2023.10.140
Received 10 March 2023; Received in revised form 18 August 2023; Accepted 12 October 2023
Available online 31 October 2023

Nomenclature

Uppercase letters

A	Absorptivity
D	Conical bluff body diameter
K	Turbulent kinetic energy
P	Thermal Load
Q_{air}	Air flow rate
Q_{fuel}	Fuel flow rate
Q_{total}	Total Flow rate
$\dot{Q}$	Average total Heat flux
S	Optical path length
S_h	Source term for combustion
T	Temperature
X	Mole fraction
Y	Mass fraction

Greek Letters

ρ	Fluid Density
α	Thermal diffusivity
τ_{ij}	Viscous stress tensor
ϵ	Turbulent dissipation rate
μ_t	Turbulent viscosity
$\dot{\omega}_y$	Unnormalized progress variable source term
Γ_y	Diffusivity
γ	Heat loss ratio
Φ	Equivalence ratio

Lowercase letters

a_k	weight factor
c	Normalised progress variable
d	Bluff body base diameter
f	Hydrogen volume fraction
f_i	Body force
h	Specific enthalpy
y	unnormalized progress variable
y_b	Unnormalized progress variable at the burnt (equilibrium state)
y_u	Unnormalized progress variable at the initial unburnt state
γ	Heat loss ratio

Subscripts

i	Component i
j	Component j
k	Specie k
avg	Average
max	Maximum

Abbreviations

LHV	Lower heating value
Slpm	Standard litres per minute
HGEN	Hydrogen enriched natural gas

temperature which facilitates thermal NO_x. However, the study compares pure methane with hydrogen enriched flame under different thermal loads for the same equivalence ratio. The hydrogen enriched flames studied have a lower thermal load and hence lower pollutant levels. On the other hand, a study conducted by Tamang et al. [12] investigates the effect of hydrogen enrichment on emissions under a constant thermal load of 50 kW while varying the equivalence ratio. The results show that for any given equivalence ratio, adding hydrogen will ultimately increase NO_x levels. The hydrogen rich fuel (90 vol%) produced more than double the amount of NOx compared to the fuel with no H_2 (0 vol%). The study also reports that hydrogen enrichment is favourable with respect to decarbonisation. Adding hydrogen drastically decreases CO_2 emissions. Furthermore, the pattern factor was included since it considers a gas turbine combustor configuration. The pattern factor alongside emissions data helped determine the optimum hydrogen enrichment which was found to be 50 vol%. The study also highlights the effect of equivalence ratio on the various flame properties. It concludes that a leaner combustion will ultimately result in lower flame temperature which explains the decrease in emission generation. Nevertheless, a leaner combustion depending on the prevailing conditions could result in poor heat transfer properties as shown by Mokheimer et al. [13]. It was concluded that for any given fuel composition, the wall temperature decreases when the amount of excess air is higher in the system.

Most studies have considered a moderate hydrogen blending of up to 45 % in natural gas. However, a numerical study conducted by Kemalettin et al. [8] investigates the effect of hydrogen enrichment by up to a level of 75 vol%. The numerical (CFD) study is conducted based on an industrial boiler system (435 kW) with a particular focus on the pollutant aspects and hence it includes both NOx and carbon emissions [8]. The addition of H_2 was found to increase NO emissions which is attributed to increase in flame temperature and hence facilitates for thermal NOx formation pathway.

The effect of hydrogen enrichment on the heat transfer capability of the flame was also investigated 14–16. Nam et al. [14] evaluates the heat transfer rate of different fuels. The study shows that hydrogen enrichment of low heating value gases (LHVG) result in lower heat transfer value. This was further attributed to a shorter flame due to its high molecular diffusivity. On the other hand, pure methane flame area is the largest and hence enhance its heat transfer property. The LHVG fuels studied by Nam et al. [14] contain N_2. The study varies H_2 levels in LHVG fuels by increasing its concentration and this simultaneously decreases N_2 levels in the fuel. Interestingly, the NOx levels did not increase with respect to hydrogen enrichment. The study finds that the effect of decreasing N_2 was almost equal to the effect of higher flame temperature due to hydrogen enrichment and hence the NOx remained unchanged. A study conducted by Piemsinlapakunchon et al. [15] numerically examined the effect of fuel hydrogen content on heat transfer capacity of laminar diffusion flames under constant co-axial air and fuel velocities. The result is in the same direction as the study by Nam et al. [14]. The heat flux at the combustion chamber wall decreases significantly with respect to H_2 and this was similarly attributed to changes in flame size. Another explanation to the decrease in heat generation capacity of the flame with respect to hydrogen enrichment was provided by Mokheimer et al. [13], in which hydrogen enrichment inhibits methane oxidation and hence producing higher levels of CO resulting in higher heat losses at the wall. This was attributed to the combustion gas residence time which is dependant on the fuel composition. The study by Piemsinlapakunchon et al. [15] also considers emission generation, and it further concludes that hydrogen enrichment of syngas increases NOx production rate as well as NOx produced per unit heat flux generated at the boundary. On the other hand, hydrogen enrichment of syngas implied lower CO_2 levels as well as less CO_2 produced per unit heat flux at the wall. The effect of hydrogen enrichment on flame charactersitics and emission generation were also investigated by several other studies as per the literatures [17–21].

The previous studies have addressed several aspects of hydrogen enriched natural gas (HGEN) fuels. However, there is little knowledge on the effect of hydrogen enrichment on premixed burners from an emission and heat generation perspective. The previous numerical (CFD) and experimental studies have mainly focused on assessing other aspects and properties of HGEN flames in several combustion systems

which encompassed flame structure, flame instability and Lewis number effect. The previous studies that examined the effect of hydrogen enrichment on the pollutant and heat transfer aspect were not based on domestic boilers and looked at other combustion systems which points out to a major knowledge gap in the literature. This study focuses on the effects of hydrogen enrichment on the pollutant and heat generation aspects of domestic boilers. Obtaining knowledge on these vital aspects will potentially enable the effective generation and utilisation of HGEN fuels in domestic heat boilers.

Therefore, in light of the above literature review and the knowledge gap identified, the key objective for this study is to investigate the impacts of fuel composition of HGEN gas with a particular focus on the heat generation and emission formation of both CO_2 and NOx. The study will also include investigation of vapour (H_2O) production since this is a crucial aspect in a burner. The study not only focuses on the effect of fuel composition but also considers the effect of combustion stoichiometry for better understanding the effective utilisation of HGEN gas. A computational fluid dynamics (CFD) model of a premixed burner is developed for this purpose and the model details are presented in the following section.

2. Model formulation

The CFD model is created based on the burner geometry of Nandula et al. [22]. An appearance and geometry of this burner is shown in Fig. 1.

Fuel and air are premixed and entrained at the base of the combustor. A conical bluff body is used to stabilise the flame with a base diameter ($D = 44.45$ mm) and an apex angle ($\alpha = 45°$). The cubic combustor test section is 79 mm × 79 mm × 284 mm. The combustor test section consists of quartz windows mounted vertically on each side.

2.1. Governing equations

The Reynolds-Averaged Navier-Stokes (RANS) is used for turbulence modelling as presented below.

Mass continuity:

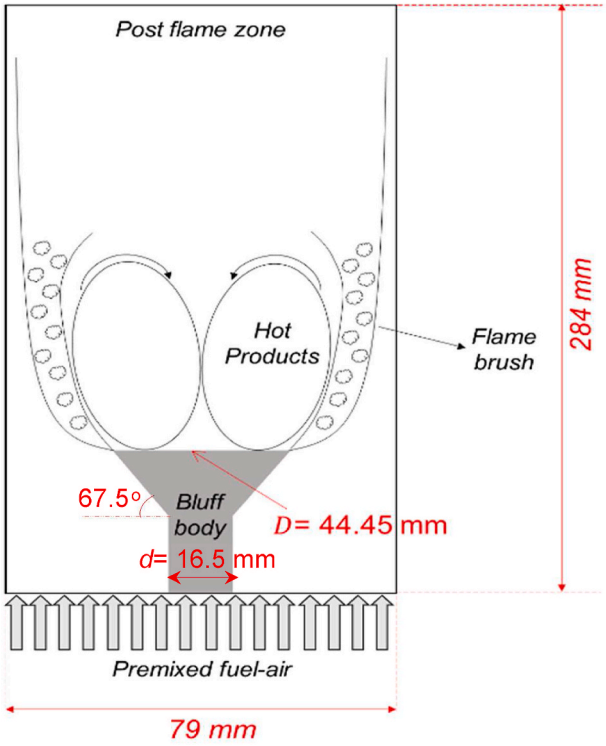

Fig. 1. Burner geometry.

$$\frac{\partial \rho}{\partial t} + \frac{\partial}{\partial x_j}\left(\rho u_j\right) = 0 \tag{1}$$

Momentum conservation:

$$\frac{\partial \rho u_i}{\partial t} + \frac{\partial}{\partial x_j}\left(\rho u_i u_j\right) = -\frac{\partial p}{\partial x_i} + \frac{\partial}{\partial x_j}\left(\overline{\tau}_{ij} - \rho \overline{u_i'' u_j''}\right) + \rho f_i, \tag{2}$$

Energy transport:

$$\frac{\partial}{\partial t}(\rho h) + \frac{\partial}{\partial x_j}\left(\rho h u_j\right) = \frac{\partial}{\partial x_j}\left(\rho \alpha \frac{\partial h}{\partial x_j} - \rho \overline{h'' u_j''}\right) + S_h \tag{3}$$

where ρ stands for the Reynolds averaged density, p denotes Reynolds averaged pressure, τ_{ij} is the viscous stress tensor, u_j are the averaged cartesian velocity components and f_i is the averaged body force. The energy equation is based on the specific enthalpy h, α denotes thermal diffusivity and S_h is the source term for combustion. The variables with $''$ stand for turbulence fluctuation components.

The standard k-epsilon model by Launder and Spalding [23] is used as a closure for RANS and the transport equations are presented below.

Turbulent kinetic energy (k):

$$\frac{\partial}{\partial t}(\rho k) + \frac{\partial}{\partial x_i}(\rho k u_i) = \frac{\partial}{\partial x_j}\left[\left(\mu + \frac{\mu_t}{\sigma_k}\right)\frac{\partial k}{\partial x_j}\right] + P_k + P_b - \rho\epsilon - Y_M + S_k \tag{4}$$

Dissipation (ϵ):

$$\frac{\partial}{\partial t}(\rho \epsilon) + \frac{\partial}{\partial x_i}(\rho \epsilon u_i) = \frac{\partial}{\partial x_j}\left[\left(\mu + \frac{\mu_t}{\sigma_\epsilon}\right)\frac{\partial \epsilon}{\partial x_j}\right] + C_{1\epsilon}\frac{\epsilon}{k}(P_k + C_{3\epsilon}P_b) - C_{2\epsilon}\rho\frac{\epsilon^2}{k} + S_\epsilon \tag{5}$$

In these equations, P_k represents the generation of turbulence kinetic energy due to the mean velocity gradients, P_b represents the generation of turbulent kinetic energy due to buoyancy. Y_M represents the contribution of the fluctuating dilatation in compressible turbulence to the overall dissipation rate. S_k is the user defined source term.

The turbulent viscosity is modelled as:

$$\mu_t = \rho C_\mu \frac{k^2}{\epsilon} \tag{6}$$

The model constants are given as:

$$C_{1\epsilon} = 1.44, C_{2\epsilon} = 1.92, C_\mu = 0.09, \sigma_k = 1.0, \sigma_\epsilon = 1.3$$

A slight modification has been done to change $C_{1\epsilon}$ from 1.44 to 1.52. This has been widely adapted in previous studies to provide a better prediction for the jet spreading rate [24].

Flamelet Generated Manifold (FGM) was used for combustion modelling. This model includes a progress variable which represents the reaction progress in order to parameterize the thermos-chemistry. The FGM model considers y which denotes the unnormalized progress variable and is defined as:

$$y = \Sigma(W_k Y_k) \tag{7}$$

where W_k is the kth species weight and Y_k is its mass fraction.

The transport equation for y is given as follows:

$$\frac{\partial \rho y}{\partial t} + \nabla \cdot (\rho u_i y) - \nabla \cdot \left(\Gamma_y \nabla y\right) = \dot{\omega}_y \tag{8}$$

where $\dot{\omega}_y$ is the unnormalized progress variable source term and Γ_y is the diffusivity which is computed from the material properties defined.

The FGM model adopts a tabulation process to solve for the mixture fraction (Z) and heat loss ratio (γ) at each point in time (t). This is then converted into the normalised progress variable (c) through the following equation

$$c = \frac{y - y_u}{y_b - y_u} \tag{9}$$

where y_u is the unnormalized progress variable at the initial unburnt state and y_b is the unnormalized progress variable at the burnt (equilibrium state).

For radiation, participating media radiation model is selected for this study. Discrete Ordinates Method (DOM) solves the radiation transport equation [25]. Weighted sum of grey gasses (WSGG) is calculated to determine the absorption coefficient. The total absorptivity of grey gasses is given below.

$$A \approx \sum_{k=0}^{K} a_k \left(1 - e^{-K_k S}\right) \tag{10}$$

where A is the absorptivity, k represents a given specie, a_k is the weight factor and S is the optical path length. The medium is assumed to be optically thin with the assumption that CO_2 and H_2O are the two most dominant gases with respect to cloud emission and absorption among all product gases from combustion [26].

2.2. Boundary conditions and mesh generation

The numerical method requires the proper computational domain and grid refinement in order to obtain the converged and reliable solution. For this burner configuration, the flame is formulated above the bluff body. Thus, the area immediately downstream of the bluff body is the volume of interest which requires a refined mesh.

The mesh pattern is designed to project the reacting flow as well as the interaction between the fluid flow and burner geometry. More cells are concentrated close to the bluff body and the axis. The higher density of cells at this location provides more accuracy for resolving the gradients by numerical method. The density of the cells slightly decreases at the higher vertical and horizontal distance from the bluff body exit. The number of cells and the distances between grids directly affect the reliability and accuracy of the result and the computational time. Thus, the mesh independency study and optimisation process are required for finding the proper mesh density for each simulation model. The directed mesh procedure in the software, which allows the on-demand design of mesh construction is utilised. A higher number of grids and cells on the computational domain provides greater detail of the solution; nevertheless, a higher computational cost is required. Three levels of mesh density (fine, medium, and coarse) are created by a hyperbolic function, and the results computed from them are compared to optimise the proper level of mesh resolution. A clustering mesh is stretched both vertically and horizontally from the outer edge of the fuel inlet tube to the pressure boundary (both top and left boundaries), axis, and co-flow air inlet. The mesh pattern is designed for computing the reacting flow field as well as the fluid interaction between the fuel inlet tube and the co-flow air stream. Different levels of mesh density have a different number of grids, cells and the smallest cell size. Details of the mesh generation for the mesh independency test are presented in Table 1. After carrying out the mesh independency test, the 'normal' mesh was found to produce identical results to the fine mesh. The 'coarse' mesh model on the other hand overpredicted the axial temperature towards the downstream, the axial temperature curve of the 'coarse' mesh model shifted upwards compared to the other two models along the downstream region. The percentage difference is given at approximately 6 %. The flame models that were generated using three different mesh resolutions were also compared with respect to H_2, N_2 and O_2 axial distributions. The 'fine' and 'normal' mesh schemes were found to produce identical result while on the other hand the 'coarse' mesh slightly overestimated O_2 and N_2 values along the domain by 2 % and 3.5 % respectively. Furthermore, the 'coarse' mesh underestimates H_2 values along the downstream by an average of 3 % compared to the other two schemes. Therefore the 'normal' mesh was chosen for this study for reduced computational cost. These results are summarised in Table 1, the fine mesh model is used as the reference case for comparison.

The boundary condition of the simulation domain is illustrated in Fig. 2. Despite the fact that the burner is a cubic combustion section, an axisymmetric domain was chosen to represent this section. The bluff body in Nandula et al. [22] experimental setup is of a conical shape and hence an axisymmetric model is an accurate representation of this important element of the burner geometry. The bluff body is the most crucial part of the geometry with respect to the effect on flow and combustion properties. Considering the experimental results which are presented in Fig. 4, it is evident that the results for temperature and all species tend to be level and constant along the far stream whereby there is no fluctuations in the values along that region. This implies that the axisymmetric model choice is justified since the flow field changes and fluctuations occur close to the bluff body and in the intermediate stream as observed in all the results that were obtained across different axial locations. The experimental results show that the walls have no effect in that respect since no change to any of the values is observed close to the wall. Combustion occurs at the temperature and pressure of 300 K and 101,325 Pa, respectively. The same temperature and pressure also apply the top boundary, which is defined as a pressure outlet. The species on these boundaries are only air, which is defined as 79 % N_2 and 21 % O_2 by volume. The bottom boundary is a mass flow inlet for the premixture. The wall boundary with non-slip and non-adiabatic conditions. The temperature at the wall is extrapolated from the solution. The height of the combustor test section (h) was extended from 284 mm to 800 mm since some simulated cases will generate a long flame and hence this modification is essential to account for longer flames.

2.3. Numerical techniques

Computational fluid dynamics (CFD) commercial code 'Star CCM +' is selected as a numerical tool to conduct this study. A segregated solver is utilised for solving the continuity, momentum, species transport, and energy transport equations. Hybrid Gauss-Least Squares Method was used for computing gradients. The methods used for calculating the dynamic viscosity and specific heat are Chapman-Enskong, and 7-coefficient NASA polynomials, respectively. The thermodynamic and transport property data are imported from the GRI3.0 mechanism database [27]. GRI 3.0 also includes NO_x formation reactions which were imported to the generated numerical models for the prediction of species distributions including NOx. The software built-in NO_x thermal model solves the transport equation for NO with the thermal source term. Thermal NO_x is formed by high temperature oxidation of atmospheric

Table 1
Mesh details.

Details of mesh dependency test									
Resolution	Levels from inlet to base of conical body	Levels from base to the end of conical body	Levels from end of conical body to the outlet	Total number of cells	Smallest cells size (mm)	Mean divergence (%)			
						Axial Distributions			
						Temperature	H_2	O_2	N_2
Coarse	20	25	500	7890	0.5	6	3	2	3.5
Normal	30	40	800	26,000	0.2	0.4	0.2	0.1	0.5
Fine	45	50	1200	55,120	0.1	Reference case			

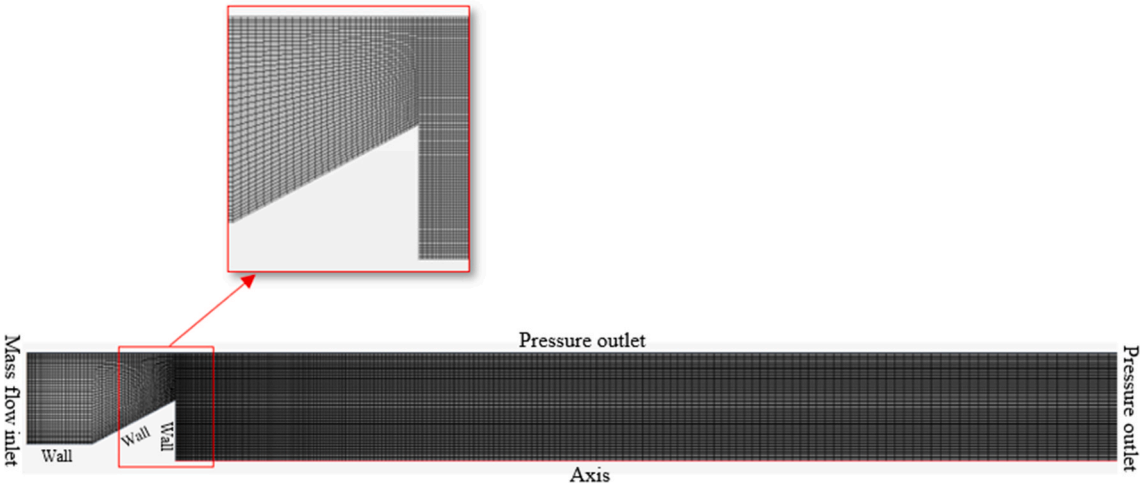

Fig. 2. Generated mesh (normal) and boundary conditions of each plane.

nitrogen. The built-in thermal NO_x model considers the three principal extended mechanisms and the corresponding reaction constants for each of the mechanisms. On the other hand, CO_2 emissions are calculated by the flamelet model whereby it is coupled with the main combustion calculations.

Molecular diffusivity and thermal conductivity are computed according to the Lewis number. The generated CFD model considers multi-component diffusion, thermal diffusion also thermal radiation. The radiation transport equation is solved by the Discrete Ordinates Method (DOM) where the absorption coefficient is calculated based on the weighted sum of grey gas model (WSGG) and the optical path length is computed. Flamelet generated manifold (FGM) is the model chosen to model chemistry-turbulence interactions. Flamelet based chemical reduction techniques are very promising methods for efficient and accurate modelling of premixed flames [28]. Over the years the Flamelet Generated Manifold (FGM) technique has been developed by the Combustion Technology Group of Eindhoven University of Technology. Current state-of-the-art of FGM for the modelling of premixed and partially-premixed flames is reviewed. The fundamental basis of FGM consists of a generalized description of the flame front in a (possibly moving) flame-adapted coordinate system. The basic nature of the generalized flamelet model is that effects of strong stretch in turbulent flames are considered by resolving the detailed structure of flame stretch and curvature inside the flame front. Details of the used methods can be found in the Star CCM + user guide [25].

The simulation was then run until convergence is obtained with a steady-state profile of the contour plots of the velocity, temperature, and concentration of major species. Residuals of continuity, momentum and energy are resulted between 10^{-4} and 10^{-6} and remained to be stable thus ensured the solution reliability and steadiness. A summary of the main numerical models is provided in Fig. 3.

3. Flame case setup

The study is based on keeping the thermal load (P) fixed at 25 kW for all the flame cases, which is typical for a domestic heating boiler [1]. The study considers different hydrogen/methane (H_2/CH_4) blends which vary with respect to the hydrogen enrichment levels. The hydrogen fraction (f) represents the amount of hydrogen present as a mole fraction and varies from 0 to 1 with an increment of 0.1, and hence there are 11 cases in each of the flame sets. The study included three flame sets which vary with respect to stoichiometry (i.e., amount of excess air). Flame set I is based on 25 % excess air which is the typical operating condition for a domestic boiler [29]. Whereas, Flame sets II and III are based on a leaner burning conditions at 37.5 % and 50 % excess air respectively. Table 2 provides the fuel properties details for the varying H_2/CH_4 blends including the Lewis number calculated based on the effective approach [8]. Details of flow conditions for the three flame sets which were

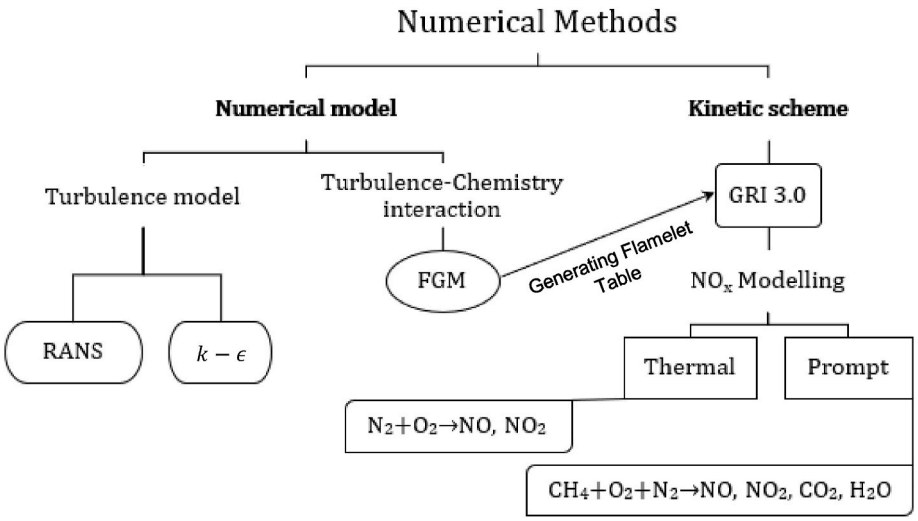

Fig. 3. Numerical method's schematic diagram.

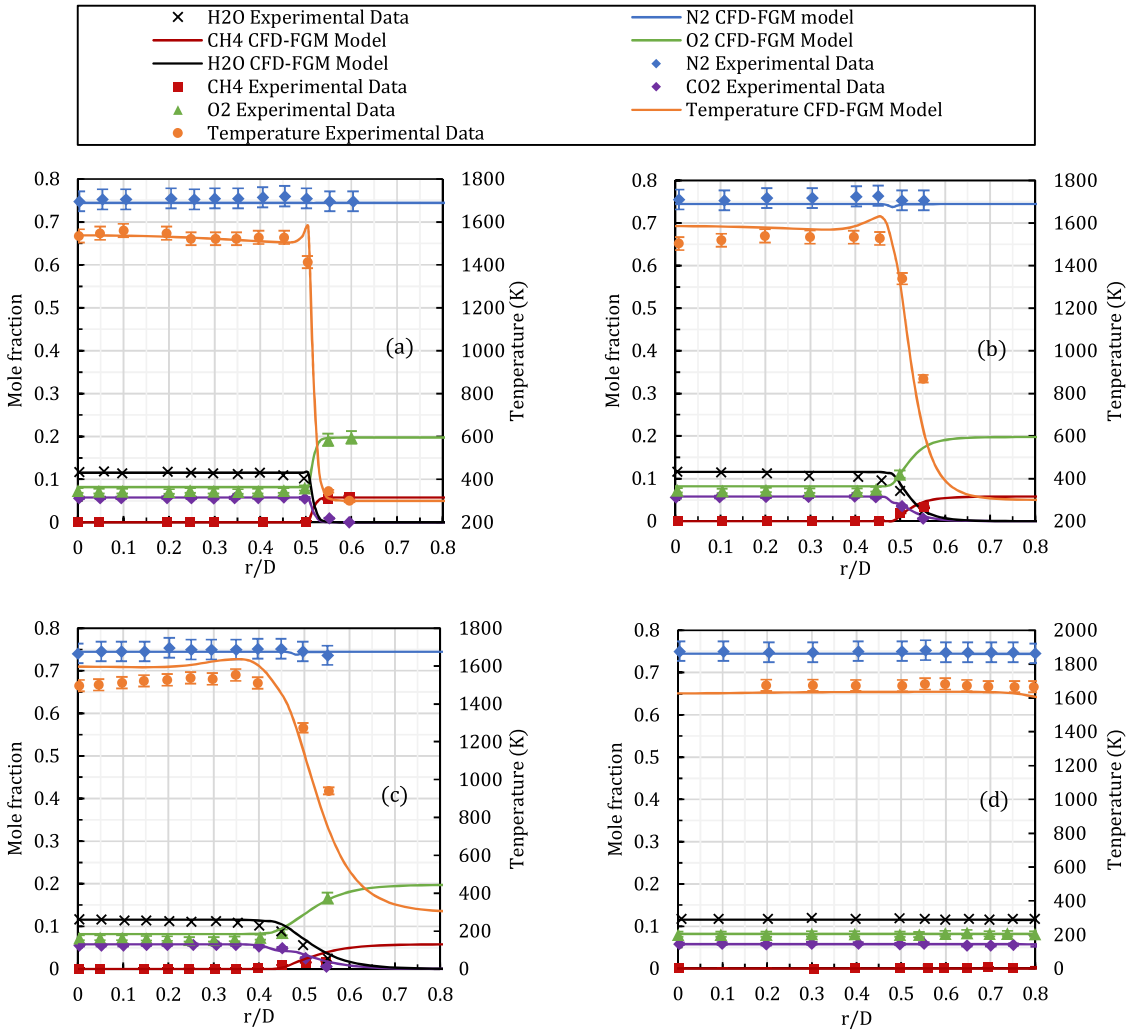

Fig. 4. Radial temperature and species profiles at (a) 0.1*D* (b) 0.6*D* (c) 1*D* and (d) 6*D* above bluff body.

Table 2
Fuel properties.

Fuel Properties			
f	ρ_{fuel} kg/m^3	LHV MJ/m^3	Lewis number
0	0.68	35.8	0.96
0.1	0.62	33.3	0.895
0.2	0.56	30.8	0.83
0.3	0.50	28.3	0.765
0.4	0.44	25.8	0.7
0.5	0.39	23.3	0.635
0.6	0.33	20.8	0.57
0.7	0.27	18.3	0.505
0.8	0.21	15.8	0.44
0.9	0.15	13.3	0.375
1	0.09	10.8	0.3

calculated based on the fuel properties and equivalence ratio (Φ) are provided in Table 3.

4. Validation of the modelling results

The burner was initially developed to experimentally investigate methane gas flow. The simulation cases are run at the similar flow condition and fuel composition as in Nandula et al. [22] in order to validate the simulation results with their experimental data. The flame parameters in the present experiment [22] correspond to an air flow rate of 3960 slpm (standard litres per minute) and fuel (CRO flow rate of 244 slpm), resulting in an equivalence ratio of 0.586. The combustor produces a cone-stabilized premised flame. The flame is stabilized by the bluff body (cone), with a recalculation zone which extends to ~ 1*D* downstream, a shear layer or an annular flame zone, and a post flame zone. Rayldgh/Raman/LIF measurements are performed at various axial and radial locations on the combustor. In addition to the optical measurements, the pollutants (CO and NO) in the exhaust plane ($x/D = 6.0$) are measured with gas sampling probes.

Computational results are compared with the experimental results of Nandula et al. [22] in Fig. 4 which represents the radial temperature and species profile of the flame. At 0.1*D*, the radial temperature is accurately predicted with its profile intersecting most experimental data points. At 0.6*D* and 1*D* above the bluff body there is a slight overprediction of temperature within the region $0 < r/D < 0.45$. At 0.6*D*, the maximum discrepancy between the experimental and numerical results for the temperature occurs at $r/D = 0.45$ and is given as 7.9 %. At 1D, the maximum discrepancy occurs at $r/D = 0.3$ and is given as 5.8 %. Overall, the margin is insignificant, and the computational result accurately predicts the position of the maximum temperature and the temperature profile shape. This implies the accuracy of the FGM method in predicting temperature at radial distances 0.6*D* and 1*D*. Furthermore, the computational result accurately predicts the temperature shape profile at a distance 6*D* from the bluff body. It also provides good quantitative agreement with an average discrepancy of only 1.8 % along the domain.

Table 3
Flow conditions for the three flame sets.

Flow conditions									
f	Flame Set I (25 % Excess air)			Flame Set II (37.5 % Excess air)			Flame Set III (50 % Excess air)		
	Q_{fuel} m^3/h	Q_{air} m^3/h	Q_{total} m^3/h	Q_{fuel} m^3/h	Q_{air} m^3/h	Q_{total} m^3/h	Q_{fuel} m^3/h	Q_{air} m^3/h	Q_{total} m^3/h
0	2.51	29.9	32.4	2.51	32.9	35.4	2.51	35.9	38.4
0.1	2.70	29.8	32.5	2.70	32.7	35.4	2.70	35.7	38.4
0.2	2.92	29.6	32.5	2.92	32.5	35.4	2.92	35.5	38.4
0.3	3.18	29.3	32.5	3.18	32.3	35.4	3.18	35.2	38.4
0.4	3.49	29.1	32.5	3.49	32.0	35.5	3.49	34.9	38.4
0.5	3.86	28.7	32.6	3.86	31.6	35.5	3.86	34.5	38.3
0.6	4.33	28.3	32.6	4.33	31.2	35.5	4.33	34.0	38.3
0.7	4.92	27.8	32.7	4.92	30.6	35.5	4.92	33.4	38.3
0.8	5.70	27.1	32.8	5.70	29.8	35.5	5.70	32.5	38.2
0.9	6.77	26.2	32.9	6.77	28.8	35.6	6.77	31.4	38.2
1	8.33	24.8	33.1	8.33	27.3	35.6	8.33	29.8	38.1

Examining the species result produced by the FGM method, the numerically produced N_2, CO_2, CH_4 and H_2O profiles intersect most experimental data points at a distance 0.1D above the bluff body. The computational result slightly overpredicts O_2 values with an average margin of 8 %. This indicates good quantitative agreement with the experiment at this height above the bluff body since the margin is insignificant. A similar trend is noticed at distances 0.6D, 1D and 6D above the bluff body. At 1D, the average discrepancy between the experimental and numerical result for O_2 is given at 11.5 %. However, at 6D above the bluff body, the computational result provides an excellent prediction for the specie O_2 since the O_2 distribution profile generated intersects most experimental data points.

A similar trend is noticed when examining the H_2O results at radial stations 0.6D and 1D. The numerical result overpredicts H_2O values along the region $0.4 < r/D < 0.5$. At 0.6D above the bluff body, the maximum discrepancy is 17 %. On the other hand, the maximum discrepancy is less significant at 0.1D and is given as 12 %.

At 0.6D above the bluff body, the maximum discrepancy between the experimental and numerical results for H_2O occurs at $r/D = 0.45$. This is also the same location at which the discrepancy is highest for temperature as mentioned previously. Hence, suggesting that an overpredicted temperature would result in an overprediction to the water vapour produced by the flame. Nevertheless, the FGM model produces an overall accurate result for H_2O distribution at both 0.6D and 1D. The average discrepancies are given as 7 % and 4 % respectively.

In conclusion, FGM model is capable of accurately solving the temperature field of a premixed turbulent flame since it provides a good prediction of the temperature profile shape in addition to providing good quantitative agreement at both the upstream and downstream regions. It also provides an accurate result for the distribution of species such as N_2, CO_2, CH_4, H_2O and O_2.

5. Results and discussion

5.1. Flame temperature and appearance

Temperature contours for pure methane ($f = 0$), equal mixture ($f = 0.5$) and pure hydrogen ($f = 1$) flames are presented in Fig. 5 for the three sets. The trend in Fig. 5 suggests that the pure hydrogen ($f = 1$) case corresponds to the largest high temperature zone in all three flame sets. The trend also suggests that switching from a pure methane fuel ($f = 0$) to an equal mixture ($f = 0.5$) results in a smaller high temperature zone. However, switching from $f = 0$ to $f = 0.5$ increases the temperature of the high temperature zone despite the reduction in size.

Fig. 6 indicates that the maximum flame temperature (T_{max}) increases with respect to the hydrogen fraction (f) in the premixture for all three flame sets. Furthermore, the results from flame set I indicate that the relationship between the maximum flame temperature (T_{max}) and

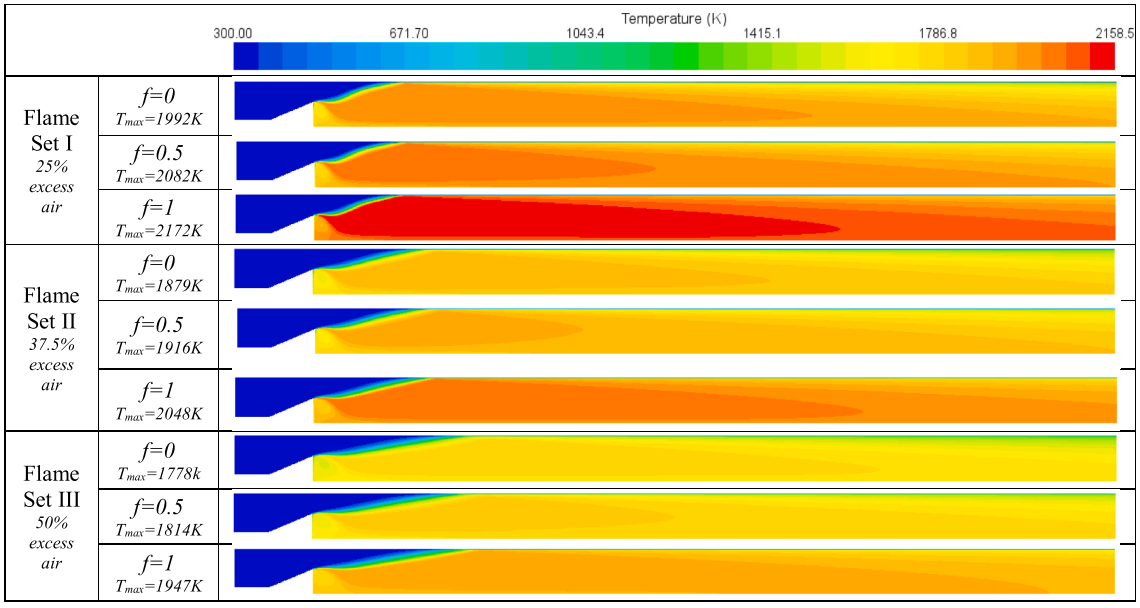

Fig. 5. Temperature contours for different flame sets.

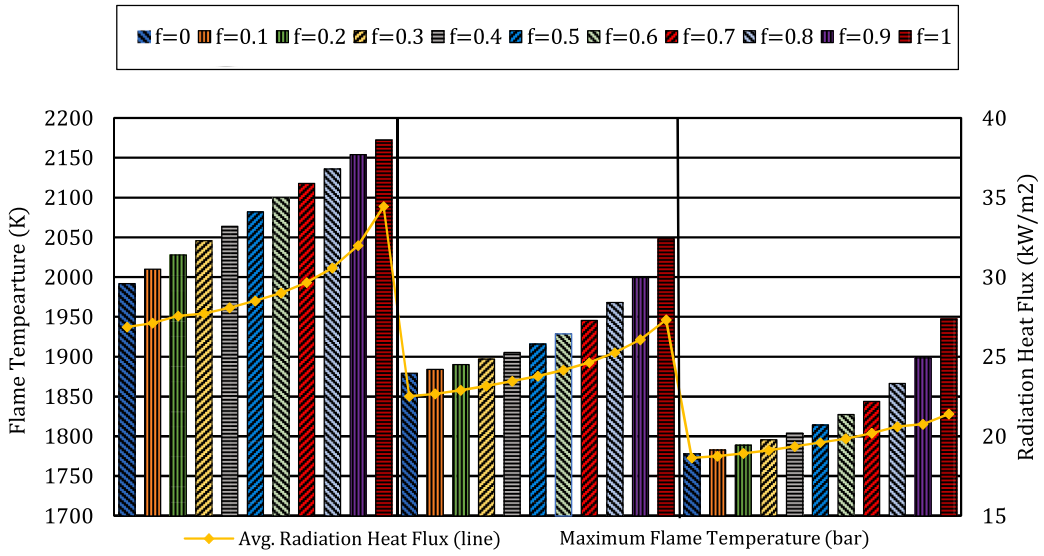

Fig. 6. Maximum flame temperature and average radiation heat flux.

hydrogen fraction (*f*) is linear unlike the two other flame cases (II & III) where these two factors are non-linearly correlated. The equivalence ratio (Φ) value determines the correlation between the maximum flame temperature (T_{max}) and hydrogen fraction (*f*) [1]. Both the equivalence ratio (Φ) and hydrogen fraction (*f*) values influence the combustion reaction properties by determining reaction coefficients for the involved species and hence flame temperature. This explains why changing the equivalence ratio at which the reaction takes place affects the type of mathematical relation between the maximum flame temperature (T_{max}) and hydrogen fraction (*f*) as observed. It is also noticed that the combustion stoichiometry has stronger effect on the flame temperature compared to the hydrogen fraction (*f*). For example, the pure methane flame ($f = 0$) in set I has a maximum temperature value ($T_{max} = 1992$ K) which is higher than the maximum temperature for pure hydrogen flame ($f = 1$) in set III.

As discussed previously, both the equivalence ratio (Φ) and the hydrogen fraction (*f*) determine the flame temperature. However, when the equivalence ratio is less than unity (i.e., Φ<1) which is the case for all the flame sets in this study, the stoichiometry of combustion has a stronger effect than the fuel hydrogen content on the combustion reaction properties [1]. Fig. 6 also provides the average radiation heat flux data for all the flame cases and the general trend suggests that the radiation heat flux increases with respect to the hydrogen fraction. This can be explained by the increase of radiative intensity occurring due to higher flame temperature [8]. Considering flame set I, the radiative heat flux increases by ~25 % while T_{max} increases by ~10 % when switching for a pure methane ($f = 0$) to a pure hydrogen ($f = 1$) fuel. The percentage increase in the radiation heat flux is less for flame set III, this is given at ~10 %. On the other hand, the percentage increase in T_{max} is constant at approximately 10 % and does not vary with respect to stoichiometry when switching from pure methane ($f = 0$) to pure hydrogen ($f = 1$). Hence, when combustion occurs with a 50 % excess air ($\Phi = 0.67$), the percentage increase in both the radiation heat flux and the flame temperature is equal at ~10 % when switching from pure methane to pure hydrogen.

5.2. Heat transfer characteristics

The total heat flux in this study represents the sum of both the conduction and radiation heat fluxes. Fig. 7 presents the profiles of total heat flux and radiation heat flux along the wall for flames in sets I, II and III. The general trend shows that as the hydrogen fraction increases, the total heat flux at any given point along the wall decreases. This further indicates that hydrocarbon (CH_4) presence has a strong role in that respect. Flame set I results in Fig. 7 (a) indicate that hydrogen addition causes the total heat flux profile to vertically shift upwards. The general trend for set I flames shows that the total heat flux reaches its peak value at a vertical distance $y = 0.07$ m above the bluff body. The result is in the same direction for flames in sets II & III. However, the main difference is that the highest value does not occur at in the immediate stream at 0.07 m. For set II flames in Fig. 7 (b), the total heat flux reaches its peak value at a distance $y = 0.16$ m above the bluff body and for set III flames Fig. 7 (c), the peak value occurs at a distance $y = 0.2$ m from the bluff body. This, therefore, suggests that varying the stoichiometry of combustion influences the location at which the highest heat generation occurs along the wall. On the other hand, varying the hydrogen fraction (*f*) does not have an effect on that aspect.

Fig. 7 also suggests that radiation becomes more significant as the hydrogen fraction increases for all the three flame sets. As seen from set I results in Fig. 7 (d), the effect of hydrogen variation becomes more significant as the fuel becomes richer with hydrogen content. The vertical distance between the profiles of $f = 0$ and $f = 0.2$ is small compared to a relatively large margin between the profiles of the two consecutive cases $f = 0.8$ and $f = 1$. When the amount of excess air is increased, the distance between the flame profiles becomes more even. This is evident when looking at the results from Set II and Set III flames in Fig. 7 (e) and (f) respectively. Therefore, increasing the air content implies a more uniform increase in the radiation heat flux along the wall with respect to the hydrogen fraction. This finding is directly linked to the temperature results discussed earlier. Radiation is strongly dependant on the flame temperature where stoichiometry plays a more important role than the fuel hydrogen concentration in determining this property. Hence, explaining why the effect of hydrogen fraction (*f*) on radiation is weakened when the amount of excess air is increased.

The average values for the total heat flux along the wall are given in Fig. 8 for all the simulated flames. The pure methane ($f = 0$) flame in set I is outstanding from the other flames with the highest average total heat flux value of 117 kW/m^2 while the lowest average heat flux value of 60 kW/m^2 corresponds to the pure hydrogen ($f = 1$) in set III. Comparing flames in set I, it is noticed that the total heat flux average value decreases in a linear manner with respect to hydrogen addition. This result is in the same direction for flames in the two other sets (II & III). As stated previously, the current maximum threshold for hydrogen enrichment is 20 % by volume ($f = 0.2$). As a result, Fig. 8 shows that the average value of the total heat flux decreases by 6 % when the volume concentration of hydrogen is increased by 20 %. This finding is based on

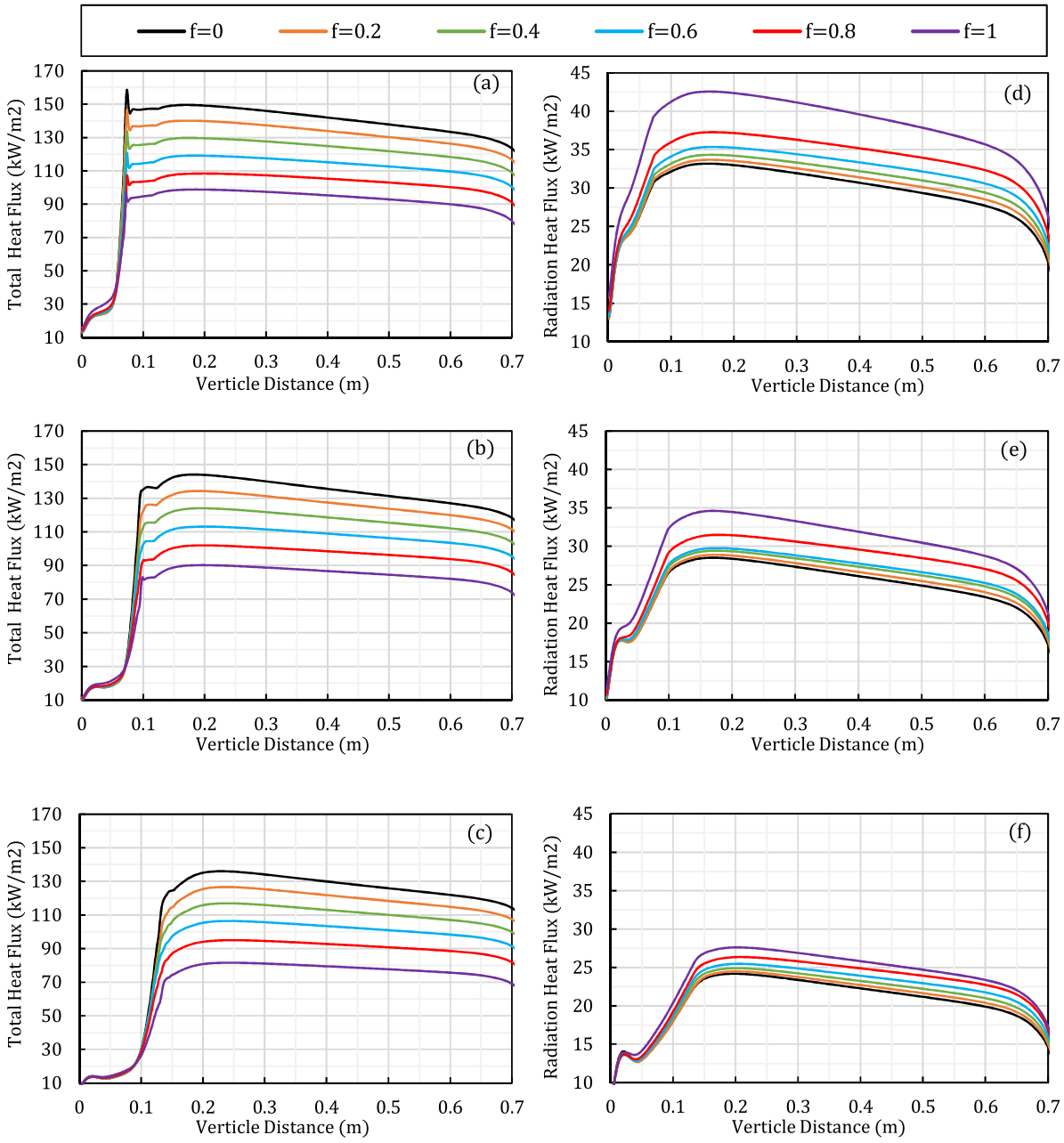

Fig. 7. Radiation and total heat flux profiles along the boundary.

the data from flame set I which is again based on a similar stoichiometry to that of a domestic boiler ($\Phi = 0.8$).

The general trend shows that making combustion leaner will result in an overall lower heat flux generated on the wall as evident in Fig. 8 when comparing the pure methane ($f = 0$) flames across the three sets. The average total heat flux value decreases by 8 % when increasing the air content from 25 % to 37.5 % and decreases further by another 9 % when the air amount increases to 50 %. Furthermore, the pure methane ($f = 0$) flame in set III generates the same heat flux as the equal mixture ($f = 0.5$) flame in set I. Both have the same average value (98 kW/m^2) which further suggests having a strong role of air content on the heat generation capability of the flame.

A more in-depth insight into the heat generation capability for each of the simulated flames is given by presenting both the conduction and radiation heat flux results in Fig. 8. The general trend shows that conduction dominates the heat transfer at the wall for all the simulated flames. The average value for the conduction heat flux decreases with respect to the hydrogen fraction (f). In all the three flame sets, the decrease in conduction heat flux as a result of higher hydrogen content (f) being present in the fuel is more significant than the increase in radiation heat flux. This explains the decrease in the average of value of the total heat flux. Fig. 8 also suggests that varying stoichiometry has a strong role on determining the nature of the heat transfer at the wall. Comparing the pure hydrogen ($f = 1$) flames from the three sets, it is noticed that increasing the air content will lead to radiation being less significant as it makes up a smaller proportion of the total heat flux. On the other hand, conduction becomes more dominant. The radiation heat flux from the pure hydrogen ($f = 1$) flame accounts for 35 %, 39 % and 43 % of the total heat flux for Set I, II & III respectively. The same trend can be found by comparing any hydrogen fraction case in Set I with its equivalent in the sets II and III.

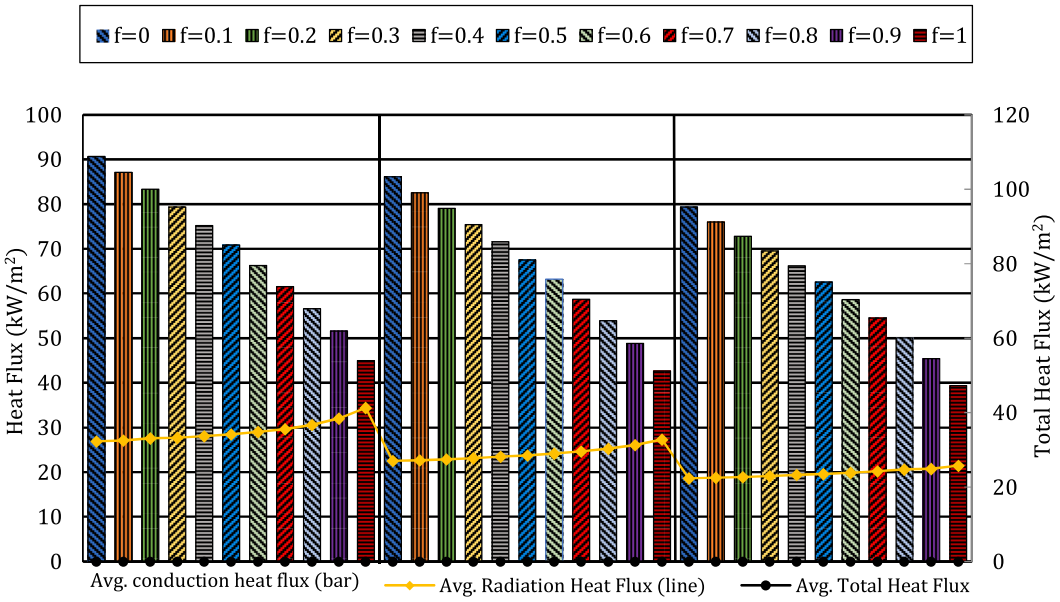

Fig. 8. Average conduction heat flux, average radiation heat flux and average total heat flux along the boundary.

5.3. Distribution of combustion species

Fig. 9 presents H_2O radial profiles at different axial stations. A similar trend appears which indicates that H_2 has a significant effect on H_2O levels. More in detail, Fig. 9 (a) which presents radial H_2O profiles at y = 0.1*D* shows the pure hydrogen (*f* = *1*) flame from set I has the highest H_2O mole fraction values at any given location in the radial direction. On the other hand, the pure methane (*f* = *0*) flame in set III produced the lowest levels of H_2O. The general trend in set I shows that for all the flames, H_2O mole fraction value is the highest at the centreline ($r = 0$) and remains at a constant value along the region $0 < r < 22$ mm followed by an abrupt decrease where H_2O tends to zero at $r > 24$ mm.

The effect of stoichiometry is also evident by examining the result from Fig. 9. At all the axial stations, the H_2O profiles of the pure methane (*f* = *0*) flame from set I and the equal mixture (*f* = *0.5*) flame from set III are very closely matched and overlap along the most regions. In this

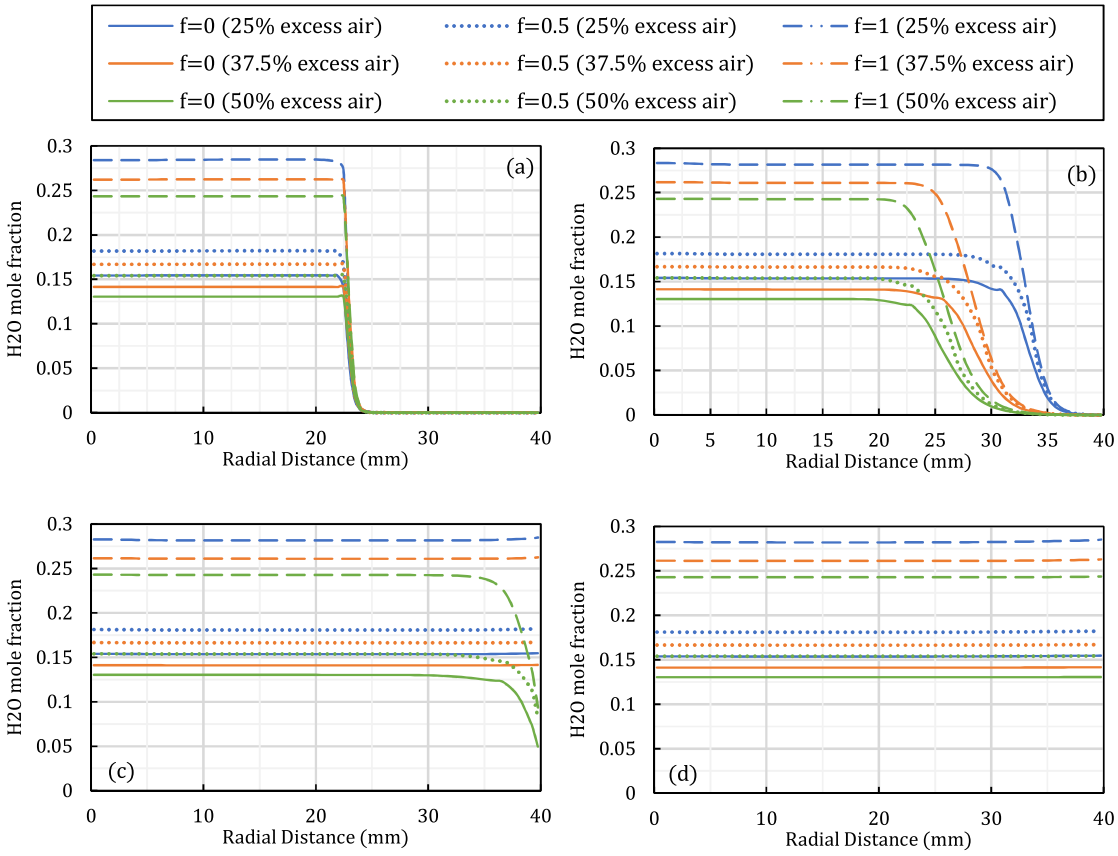

Fig. 9. H_2O radial profiles (a) 0.1D (b) 1D (c) 3D (d) 6D from bluff body.

case, the effect of increasing hydrogen content by 50 % is equal to the effect of increasing the amount of excess air by 25 % on H_2O levels. However, at $y = 1D$ the pure methane flame ($f = 0$) from set I has significantly higher H_2O mole fraction values in the far stream ($r > 25$ mm) compared to the equal mixture ($f = 0.5$) flame from set III.

Fig. 10 (a) which presents CO_2 results at a distance $y = 0.1D$ from the base of the bluff body indicates a general trend. CO_2 mole fraction value is constant along the region ($0 < r < 23$ mm) and abruptly decreases beyond this range where it tends to zero at the far stream. At all the axial locations, the general trend shows that CH_4 holds a strong role with respect to CO_2 levels. Higher methane fuel content results in an increase to CO_2 levels. The result at axial station $y = 0.1D$ shows that increasing the amount of excess air is an effective strategy to reduce CO_2 levels. However, the effect of fuel species (CH_4:H_2) on CO_2 levels is more significant than stoichiometry with respect to CO_2 levels. This finding can be observed at all the axial stations where the equal mixture ($f = 0.5$) flame from set I produces lower CO_2 levels compared to the pure methane ($f = 0$) flame from set III. Hence, reducing the methane fuel content by 50 vol% results in lower CO_2 levels despite the combustion being carried out in more fuel-rich condition. This emphasises the role of hydrocarbon fuel presence (i.e., methane) since its reaction pathway facilitates CO_2 formation.

Examining the CO_2 results at the axial station $y = 1D$ in Fig. 10 (b), it is noticed that for set I flames CO_2 is highly present close to the bluff body and remains at a constant level up until 28 mm away from the base of the bluff body in the radial direction. Beyond 28 mm, CO_2 mole fractions gradually decrease and tend to zero near the wall. On the other hand, Flames in set II and set III produce the highest CO_2 levels along the region ($0 < r < 23$ mm) and ($0 < r < 20$ mm) respectively. At this axial station ($y = 1D$), as the combustion becomes leaner the location at which the CO_2 levels begin to decline is closer to the base of the bluff body in the radial direction. It is observed that at the axial station ($y = 1D$), the CO_2 mole fraction values of the pure methane ($f = 0$) flame from Set III are lower than those of the hydrogen rich flame ($f = 0.9$) from set I at any given location along the region (26 mm $< r <$ 40 mm). Nevertheless, the pure methane flame from set III produces overall higher CO_2 levels compared to the hydrogen rich ($f = 0.9$) flame from set I when considering the whole domain from the centreline ($r = 0$ mm) to the wall. The role of CH_4 is more important in the close and intermediate streams while on the other hand the stoichiometry of combustion becomes more significant in the far stream near the wall. This further implies that overall, the fuel composition (CH_4:H_2) has the strongest influence on CO_2 levels.

Looking at the radial NO mole fraction profiles at different axial stations in Fig. 11, a trend appears across all the axial stations which indicates that H_2 has a significant effect on NO levels. More in detail, Fig. 11 (a) which presents results at axial location $y = 0.1D$ shows that the highest NO mole fractions values correspond to the pure hydrogen ($f = 1$) flame from set I while on the other hand the pure methane ($f = 0$) flame from set III has the lowest NO mole fraction values along most of the region. The general trend shows that for all the flames, the NO mole fraction value is at its second highest value at the centreline ($r = 0$ mm) and then decreases gradually along the region ($0 < r < 10$ mm). It then remains constant along the region ($10 < r < 20$ mm) which is followed by a sudden increase to reach its peak value at approximately $r = 22$ mm for all flames. It is also noticed that the NO mole fraction profiles of the equal mixture ($f = 0.5$) flame in set II and the pure methane ($f = 0$) flame in set I are very closely matched since they overlap along most of the region. This suggests that despite an increase in hydrogen content (vol %) by 50 %, increasing the excess air by 12.5 % kept the NO levels unchanged which implies that making the combustion leaner is an effective way to combat the effects of hydrogen enrichment with respect to NO_x emissions.

The NO radial profiles at $y = 1D$ is slightly different compared to the result at $y = 0.1D$. More in detail, it is noticed that the equal mixture ($f =$ 0.5) flame from set I has higher NO mole fraction values than the pure

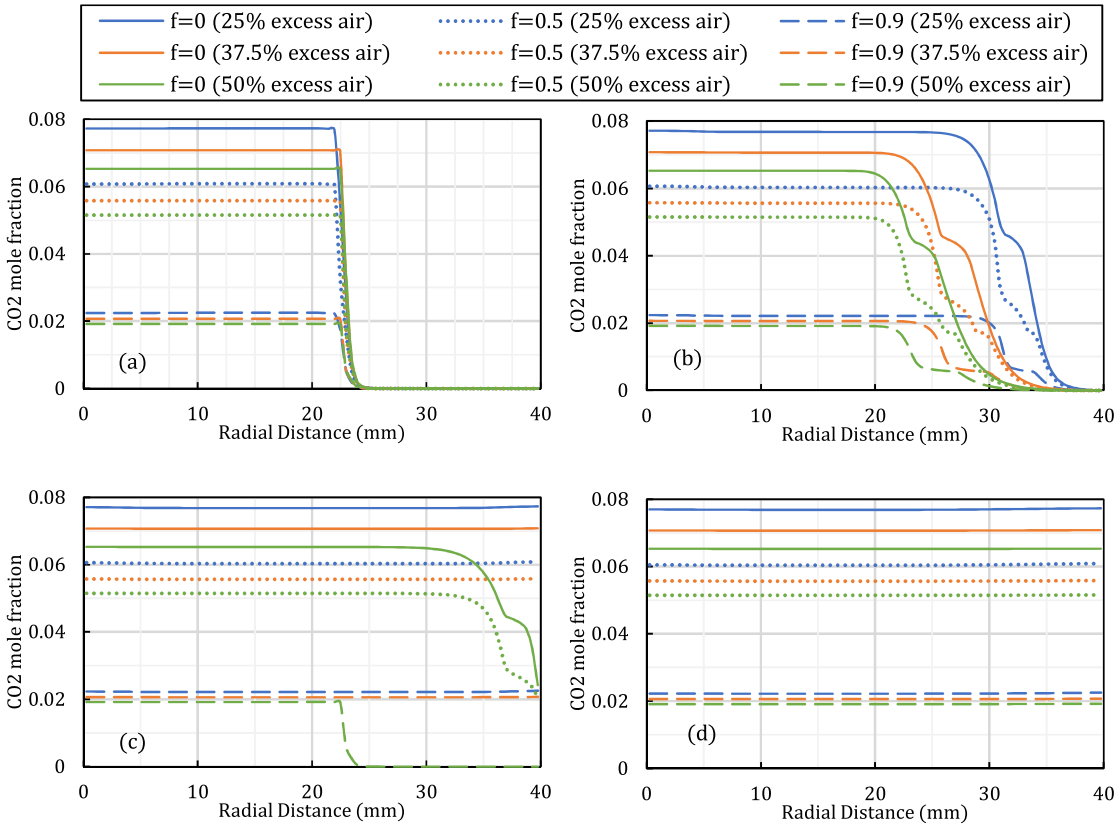

Fig. 10. CO_2 radial profiles (a) 0.1D (b) 1D (c) 3D (d) 6D from bluff body.

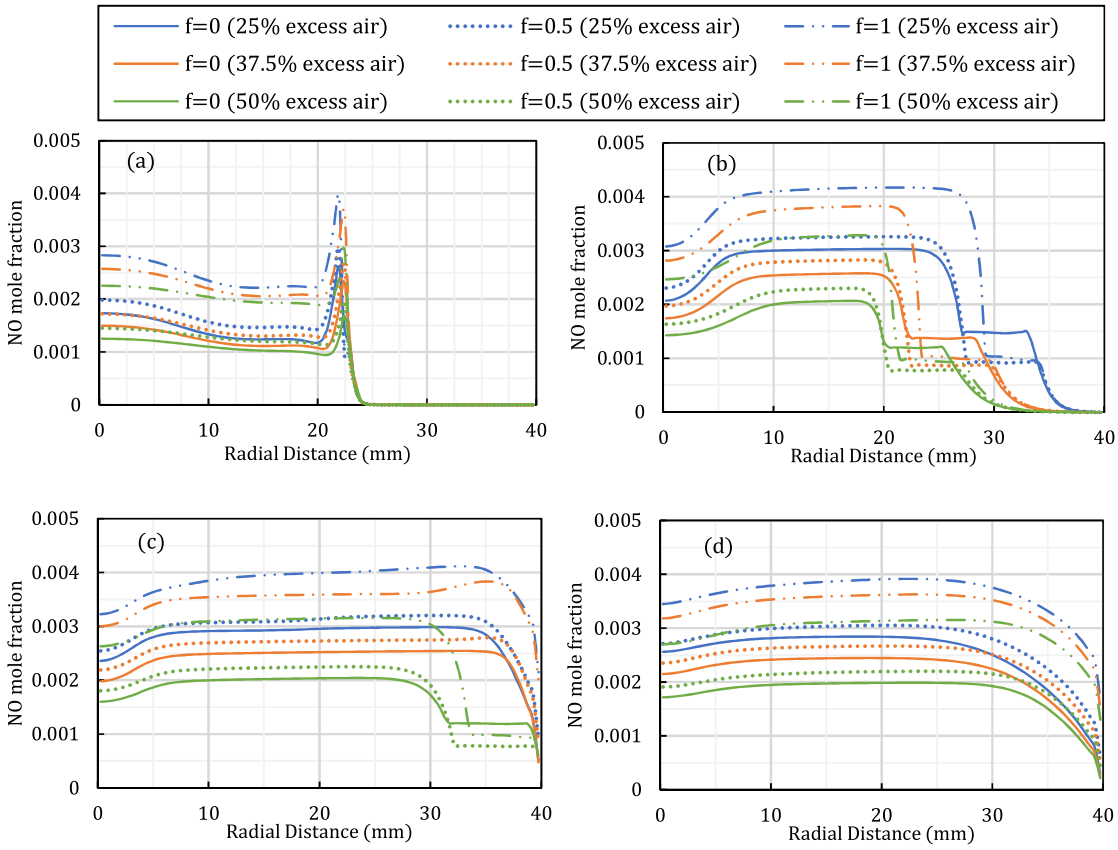

Fig. 11. NO radial profiles (a) 0.1D (b) 1D (c) 3D (d) 6D from bluff body.

hydrogen ($f = 1$) flame from set III along most of the region. This further provides an insight into understanding the significant role of stoichiometry with respect to NO emission generation. Focusing on flames from set I, it is noticed that the pure hydrogen ($f = 1$) flame has significantly higher NO mole fraction values along most of the domain ($0 < r < 28$ mm) when compared to the pure methane ($f = 0$) flame. Nevertheless, the pure methane ($f = 0$) flame has higher NO mole fraction values in the far stream ($28 < r < 40$ mm) compared to both the pure hydrogen ($f = 1$) and the equal mixture ($f = 0.5$) flames in set I. A similar trend is noticed for flames in set II and III at this axial station ($y = 1D$).

The NO radial results at $y = 3D$ and $y = 6D$ in Fig. 11 (b) and (c) respectively show that the NO mole fraction profiles of the equal mixture ($f = 0.5$) flame in set I and the pure hydrogen ($f = 1$) flame in set III are very closely matched since they overlap along most of the region. However, at axial station y = 6D the pure hydrogen ($f = 1$) flame in set III has higher NO mole fraction values than the equal mixture ($f = 0.5$) flame in set I in the far stream ($r > 23$ mm). This is contrary to the findings at axial stations $y = 1D$ and $y = 3D$ where the NO mole fraction values are lower in the far stream. At axial locations $y = 1D$, $y = 3D$ and $y = 6D$, it is also evident that the pure methane ($f = 0$) from set I has slightly higher NO mole fraction values than the equal mixture ($f = 0.5$) flame from set II along most of the domain. This further emphasises the role of stoichiometry.

5.4. Emission and vapour generation

In this section, the emission and vapour quantities are provided as a function of the burner's thermal load. Hence H_2O, CO_2 and NO_x levels are indicated by the sum of concentration divided by the thermal output which is constant for all cases (25 kW). This allows for comparisons to be drawn on efficiency basis.

Fig. 12 (a) provides the result for the total H_2O concentration per unit output. Water production is a vital aspect of burner design and is one of the key factors in determining the potential of *HGEN* fuels being utilised in boilers. The general trend across all three sets suggests that increasing H_2 fraction significantly increases H_2O levels in a non-linear manner. This is attributed to the H_2 reaction pathway which involves H_2O production. Focusing on flames from set I, it is noticed that the percentage increase in overall H_2O level is 15 % when switching from a pure methane ($f = 0$) to an equal mixture ($f = 0.5$) flame. On the other hand, the percentage increase in overall H_2O level is 44 % when switching from an equal mixture ($f = 0.5$) to a pure hydrogen ($f = 1$) flame. This finding indicates that the effect of H_2 becomes more significant as the flame becomes more enriched and CH_4 concentration in the fuel decreases. A similar trend is noticed when examining each of the other flame sets separately. Fig. 12 also indicates that stoichiometry affects the overall H_2O concentration levels for a flame. Comparing the pure methane ($f = 0$) across the three sets that vary with respect to stoichiometry. [H_2O]: P values (kmol/kWm^3) are 0.82.0.78 and 0.74 for Set I, II and III respectively. The percentage difference between Set III and Set I values is given at 9 %. Furthermore, the percentage decrease in overall NOx emissions when increasing excess air from 25 % (set I) to 50 % (set III) is also given at approximately 9 % for equal mixture ($f = 0.5$) and pure hydrogen ($f = 1$) flames. Hence, stoichiometry effect on H_2O appears to be constant with respect to hydrogen enrichment since at any given hydrogen fraction (f) increasing excess air by 25 %, resulting in a 9 % decrease in the overall H_2O concentration levels.

Fig. 12 (b) considers the whole domain and presents the CO_2 molar concentration data for the whole burner. This is the main point of interest with respect to CO_2 emission generation since it considers a whole flame. By referring to Fig. 12 (b), it is noticed that the highest overall CO_2 emissions per unit thermal output (0.016 kmol/kWm^3) are generated by the pure methane flame ($f = 0$) in Set I while on the other hand the lowest overall CO_2 emissions per unit output (0 kmol/kWm^3)

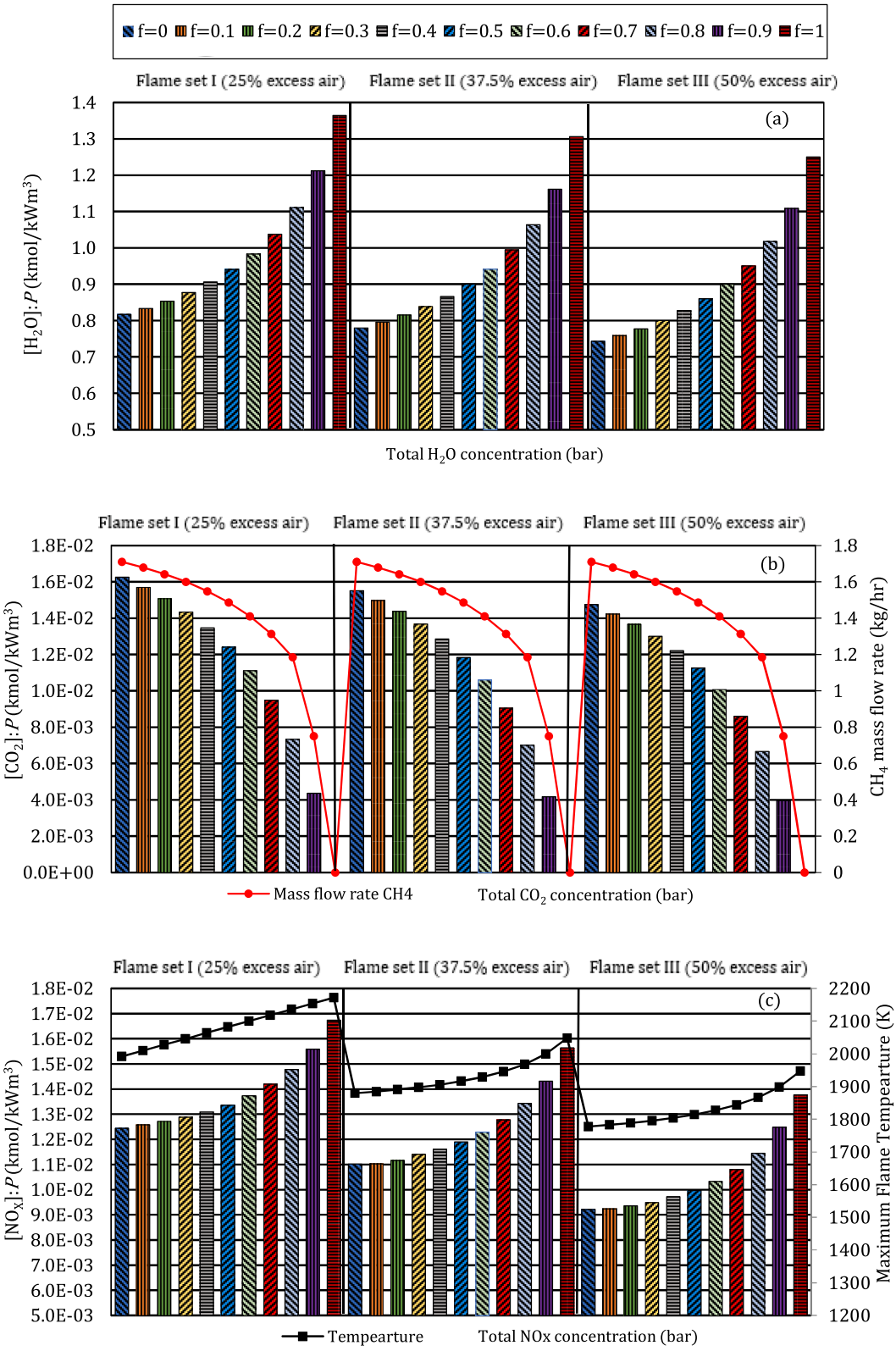

Fig. 12. Sum of Molar concentrations for all simulated cases, (a) H_2O, (b) CO_2, (c) NO_x.

correspond to the pure hydrogen flame ($f = 1$) in any of the three sets. Fig. 12 (b) also shows the correlation between the amount of CH_4 in the fuel being combusted (i.e. CH_4 mass flow rate kg/hr) and the CO_2 levels for each of the flames. The general trend shows that as the amount of CH_4 decreases the overall CO_2 levels significantly decrease. Considering Set I flames, it is noticed that the percentage decrease in overall CO_2 level is 20 % when switching from a pure methane ($f = 0$) to an equal mixture ($f = 0.5$) flame. On the other hand, the percentage decrease in overall CO_2 level is 62.5 % when switching from an equal mixture ($f = 0.5$) to a hydrogen rich ($f = 0.9$) flame. This finding indicates that the

effect of fuel composition (H_2:CH_4) becomes more significant as the flame becomes more hydrogen rich. Also, a similar trend is noticed when examining each of the other flame sets separately. The effects of stoichiometry are also observed. When comparing the pure methane ($f = 0$) flame across the three sets that vary with respect to stoichiometry, CO_2 molar concentration values for a unit output (kmol/kWm^3) are 0.0160, 0.0155 and 0.0049 for Set I, II and III respectively. Hence, increasing the excess air content by 25 % corresponds to a relatively small percentage decrease of 10 % in overall CO_2 levels. Furthermore, comparing the rich hydrogen ($f = 0.9$) flame from Set III to its equivalent in set I. The percentage decrease in overall CO_2 levels is also given at approximately 10 % which suggests that the effect of varying stoichiometry is constant throughout unlike the effect of fuel species concentration (H_2:CH_4) which becomes more significant with respect to hydrogen enrichment.

Fig. 12 (c) considers both NO and NO_2 emissions as a function of flame temperature for all the simulated cases. The general trend across all three sets suggests that increasing H_2 fraction significantly increases the total NO_x concentration for a unit output generated in a non-linear manner. This is attributed to the increase in flame temperature and hence underlines the strong role of thermal NO_x formation. Considering Set I results, it is noticed that the percentage increase in overall NO_x level is 7.25 % when switching from a pure methane ($f = 0$) to an equal mixture ($f = 0.5$) flame. On the other hand, the percentage increase in overall NO_x level is 25.7 % when switching from an equal mixture ($f = 0.5$) to a pure hydrogen ($f = 1$) flame. This finding indicates that the effect of H_2 effect becomes more significant as the flame becomes more enriched. A similar trend is noticed when examining each of the other flame sets separately. Fig. 12 (c) also indicates that stoichiometry affects the overall NO_x concentration levels for a flame. Comparing the pure methane ($f = 0$) across the three sets that vary with respect to stoichiometry. NO_x:P (kmol/kWm^3) values are 0.0124, 0.011 and 0.009 for Set I, II and III respectively. The percentage difference between Set III and set I values is given at 26 %. Recall that the percentage difference was 10 % for CO_2 concentration levels in Fig. 12. This shows that stoichiometry has a significantly stronger effect on NO_x compared to CO_2 emission generation. Furthermore, the percentage decrease in overall NOx emissions when increasing excess air from 25 % (set I) to 50 % (set III) is given at 26 % and 34 % for equal mixture ($f = 0.5$) and pure hydrogen ($f = 1$) flames respectively. Therefore, stoichiometry has a stronger effect as the flame becomes more hydrogen enriched.

5.5. Emissions per unit heat flux

It is evident that there is a trade-off between the flame performance and emission generation. Hence, the ratio between heat flux and emissions for each of the flames was calculated to provide a better understanding on the trade-off. Fig. 13 (a) presents results of CO_2 emissions per unit heat flux generated. This is obtained through dividing the sum

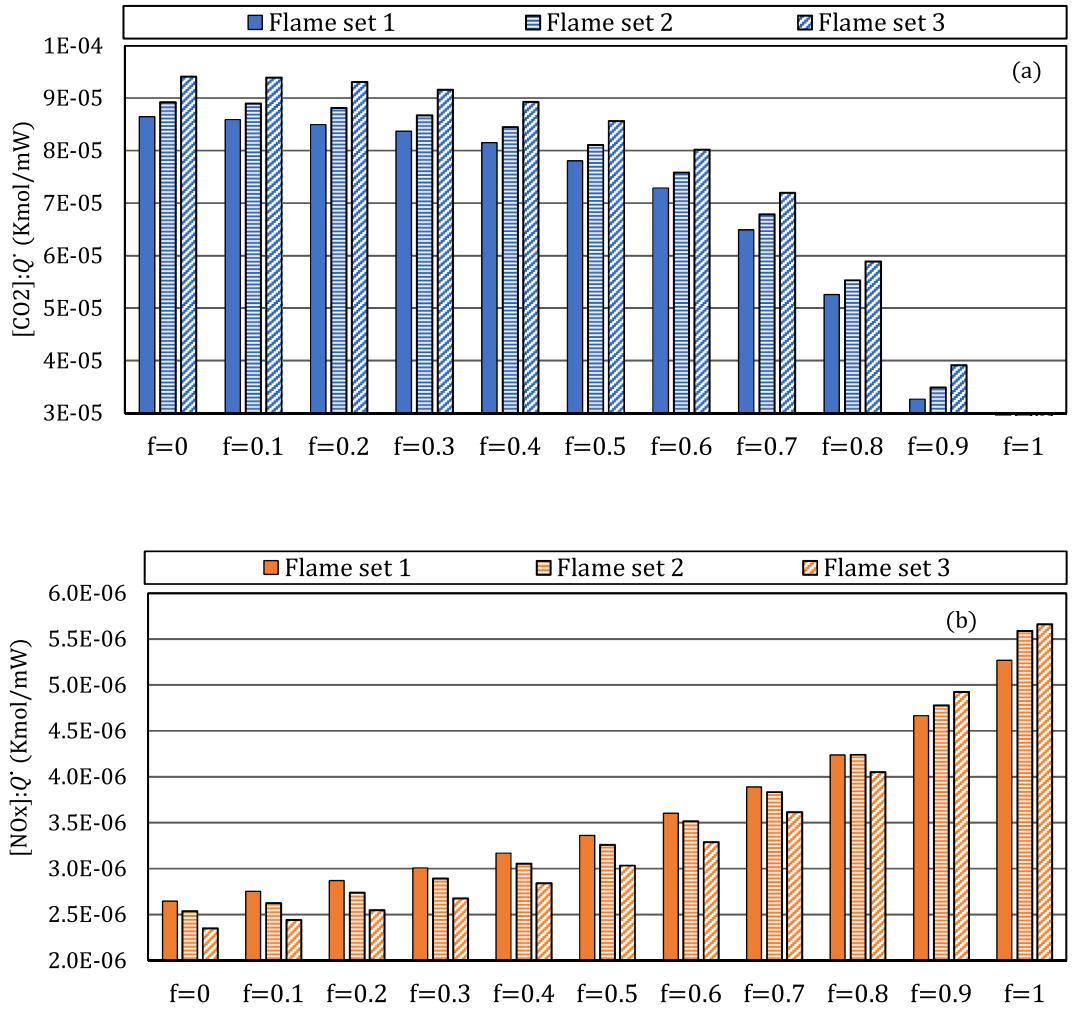

Fig. 13. Species concentration for 1 W-m^{-2} of Heat Flux generated, (a) CO_2 (b) NOx.

of CO_2 molar concentration by the average unit heat flux generated on the boundary for each of the flames.

The results from Fig. 13 (a) indicate that as the hydrogen fraction increases less CO_2 emissions are produced for a unit heat flux. Considering Set I for example, the [CO_2]: $\dot{Q}$ decreases by 12 % when switching from a pure methane ($f = 0$) fuel to an equal mixture ($f = 0.5$). [CO_2]: $\dot{Q}$ decreases by a more significant amount (58 %) when hydrogen concentration in the fuel is increased to reach $f = 0.9$. This indicates that despite hydrogen enrichment decreasing the average heat flux at the boundary, the decrease in CO_2 levels is proportionally higher thus resulting in a lower [CO_2]: $\dot{Q}$ value. Fig. 13 (a) also underlines the effect of stoichiometry on [CO_2]: $\dot{Q}$. At any equal hydrogen fraction (f), increasing the amount of excess air will increase [CO_2]: $\dot{Q}$. At $f = 0$ (pure methane), it is noticed that increasing the excess air from 25 % (Set I) to 50 % (set III) will increase [CO_2]: $\dot{Q}$ by 9 %. Furthermore, the percentage increase in [CO_2]: $\dot{Q}$ when increasing excess air from 25 % (set I) to 50 % (set III) is given at 9 % and 13 % for equal mixture ($f = 0.5$) and hydrogen rich ($f = 0.9$) flames respectively. Therefore, carrying out the combustion at 25 % (set I) which is typical in real-life applications results in the least carbon emission generated for a unit heat flux at any given hydrogen fraction.

Fig. 13 (b) presents results of NO_x emissions per unit heat flux generated. The results indicate that as the hydrogen fraction decreases, higher NO_x emissions are produced for a unit heat flux. Despite hydrogen enrichment being an effective strategy in reducing CO_2 emissions, the higher NO_x levels represent a challenge. [NO_x]: $\dot{Q}$ increases by 30 % when switching from a pure methane ($f = 0$) fuel to an equal mixture ($f = 0.5$). Recall that [CO_2]: $\dot{Q}$ decreased by only 12 %. Furthermore, [NO_x]: $\dot{Q}$ increases by a significant 56 % when switching from equal mixture ($f = 0.5$) to a pure hydrogen ($f = 1$) flame. Contrary to [CO_2]: $\dot{Q}$ results, making the combustion leaner will result in lower [NO_x]: $\dot{Q}$ up until the hydrogen fraction (f) is 0.8. This is attributed to the decrease in flame temperature which will result in lower thermal NO_x formation. Fig. 8 also suggests that the average total heat flux at the boundary will decrease as the combustion becomes leaner. However, the decrease in NO_x is more significant and hence this results in a lower [NO_x]: $\dot{Q}$ value. Nevertheless, when $f > 0.8$ the reduction in heat flux becomes more significant than NOx and hence this leads to a higher [NO_x]: $\dot{Q}$ value when the combustion becomes leaner. At $f = 0$ (pure methane), it is noticed that increasing the excess air from 25 % (Set I) to 50 % (set III) will decrease NO_x: $\dot{Q}$ by 4 %. Furthermore, the percentage difference in [NO_x]: $\dot{Q}$ when increasing excess air from 25 % (set I) to 50 % (set III) is given at −12 % and +8 % for equal mixture ($f = 0.5$) and pure hydrogen ($f = 0.1$) flames respectively. Hence, making the combustion leaner is an effective strategy to reduce [NO_x]: $\dot{Q}$ given that hydrogen fraction $f \leq 0.8$. However, it will also significantly increase [CO_2]: $\dot{Q}$ which underlines the trade-off between carbon and NOx emissions in this study.

6. Conclusions

The effect of hydrogen enrichment in HGEN fuels defined by the fuel hydrogen fraction (f) in addition to the effect of combustion stoichiometry on various flame properties has been studied. The results obtained from this study indicated that the hydrogen fuel content (f) which controls the level of hydrogen enrichment and the combustion equivalence ratio (Φ) which controls stoichiometry played an important role in determining the flame properties such as the flame temperature, heat flux, H_2O production in addition to CO_2 and NO_x emissions. It was found that stoichiometry had a different level of influence on the flame properties compared to the fuel composition (H_2:CH_4). Varying the stoichiometry of combustion to make it leaner had an undesirable effect of increasing CO_2 for a unit heat flux generated. The findings from this study could be used to determine the potential and viability of HGEN use in domestic boilers.

The key finding of this study further showed that enhancing the heat generation capability of a domestic boiler flame comes at the expense of increased CO_2 and NO_x emissions. These undesirable combustion products are a price to pay for heat generation. Therefore, the study focused on the trade-off between the heat flux and the emission generation. During the analysis of the obtained computational results, the effect of hydrogen enrichment was pointed out. It was evident that hydrogen enrichment is a very effective strategy in reducing CO_2 emissions per heat flux. However, this comes at the expense of higher NOx emissions as well as an increase in NO_x production for the same amount of heat generated which represents the main challenge.

The most favourable conditions for the premixed combustor in this study were observed when hydrogen enrichment is at 70 vol% and equivalence ratio of 0.8. These conditions yielded relatively high wall heat flux, significantly lower carbon emissions without a drastic increase in NO_x generation. Introducing 70 vol% H_2 reduces CO_2 emission levels by a 44 % while decreasing the average wall heat flux by 31 %. Hence, its impact on the heat transfer capacity is less significant than its ability to reduce carbon emissions. Furthermore, at this hydrogen blend, NOx was kept at a relatively close level to fuels with lower hydrogen content without a significant increase occurring. 70 vol% H_2 also happens to be the intersection point between [CO_2]: $\dot{Q}$ and [NO_x]: $\dot{Q}$. However, 70 vol % H_2 is only optimum if we consider the NO_x and CO_2 emissions to be equally significant. In addition, H_2O production from high levels of enrichment could imply that a hydrogen concentration of 70 % vol is not a viable option. Current government regulations do not allow for enrichment levels higher than 20 % vol and there are also other factors such as storage, explosiveness hazard, cost and infrastructure which have not been considered in this study.

Data availability

All data supporting this study will be available from the corresponding author upon reasonable request.

Declaration of competing interest

The authors declare that they have no known competing financial interests or personal relationships that could have appeared to influence the work reported in this paper.

Acknowledgements

MCP acknowledges support from Engineering and Physical Sciences Research Council (EPSRC) [EP/T022701/1, EP/N020472/1]; Network-H2 Flex Transport grant – EPSRC/Durham (NH2-006); Energy Technology Partnership (ETP) (PR008-HE).

References

[1] Schiro F, Stoppato A, Benato A. Modelling and analyzing the impact of hydrogen enriched natural gas on domestic gas boilers in a decarbonization perspective. Carbon Res Conversion 2020;3:122–9.
[2] Jones DR, Al-Masry WA, Dunnill CW. Hydrogen-enriched natural gas as a domestic fuel: an analysis based on Flash-back and blow-off limits for domestic natural gas appliances within the UK Sustainable. Energy Fuel 2018;2(4):710–23.
[3] Zhang M, et al. Flame front structure and burning velocity of turbulent premixed CH4/H2/Air Flames. Int J Hydrogen Energy 2013;38(26):11421–8.
[4] Vargas AC, et al. Burning velocity of turbulent methane/air premixed flames in subatmospheric environments. ACS Omega 2020;5(39):25095–103.
[5] Barlow RS, Dunn MJ, Magnotti G. Preferential transport effects in premixed bluff-body stabilized CH4/H2 Flames. Combust Flame 2015;162(3):727–35.
[6] Dunn MJ, Barlow RS. Effects of preferential transport and strain in Bluff Body stabilized lean and rich premixed CH4/Air Flames. Proc Combust Inst 2013;34(1):1411–9.
[7] Chakraborty N, Cant RS. Effects of lewis number on turbulent scalar transport and its modelling in turbulent premixed flames. Combust Flame 2009;156(7):1427–44.

[8] Dinkelacker F, Manickam B, Muppala SPR. Modelling and simulation of lean premixed turbulent methane/hydrogen/air flames with an effective Lewis number approach. Combust Flame 2011;158(9):1742–9.
[9] Kutkan H, et al. Modeling of turbulent premixed CH4/H2/air flames including the influence of stretch and heat losses. J Eng Gas Turbines Power 2021;144(1).
[10] Boulahlib MS, Medaerts F, Boukhalfa MA. Experimental study of a domestic boiler using hydrogen methane blend and fuel-rich staged combustion. Int J Hydrogen Energy 2021;46(75):37628–40.
[11] Pignatelli F, et al. Pilot impact on turbulent premixed methane/air and hydrogen-enriched methane/Air Flames in a laboratory-scale gas turbine model combustor. Int J Hydrogen Energy 2022;47(60):25404–17. https://doi.org/10.1016/j.ijhydene.2022.05.282.
[12] Tamang S, Park H. An investigation on the thermal emission of hydrogen enrichment fuel in a gas turbine combustor. Int J Hydrogen Energy 2023. https://doi.org/10.1016/j.ijhydene.2023.07.144. Preprint.
[13] Mokheimer EM, Sanusi YS, Habib MA. Numerical study of hydrogen-enriched methane-air combustion under ultra-lean conditions. Int J Energy Res 2016;40(6):743–62. https://doi.org/10.1002/er.3477.
[14] Nam HT, Lee S, Jung H. Effect of hydrogen addition on combustion and thermal characteristics of impinging non-premixed jet flames for various heating value gases. Case Stud Therm Eng 2023;49:103173. https://doi.org/10.1016/j.csite.2023.103173.
[15] Piemsinlapakunchon T, Paul MC. Effects of fuel compositions on the heat generation and emission of syngas/producer gas laminar diffusion flame. Int J Hydrogen Energy 2019;44(33):18505–16. https://doi.org/10.1016/j.ijhydene.2019.05.178.
[16] Belhaj Brahim MM, et al. Numerical Study of hydrogen enrichment effects in oxy-flame turbulent of three separated Jets. Appl Therm Eng 2017;113:490–8.
[17] Büyükakın MK, Öztuna S. Numerical investigation on hydrogen-enriched methane combustion in a domestic back-pressure boiler and non-premixed burner system from flame structure and pollutants aspect. Int J Hydrogen Energy 2020;45(60):35246–56.
[18] Pignatelli F, et al. Pilot impact on turbulent premixed methane/air and hydrogen-enriched methane/Air Flames in a laboratory-scale gas turbine model combustor. Int J Hydrogen Energy 2022;47(60):25404–17.
[19] Rahimi S, et al. The effect of hydrogen addition on methane-air flame in a stratified Swirl Burner. Energy; 2022. p. 126354.
[20] Liu Z, et al. Effects of hydrogen addition on combustion characteristics of a methane fueled mild model combustor. Int J Hydrogen Energy 2022;47(36):16309–20.
[21] Meloni R, Nassini PC, Andreini A. Model development for the simulation of the hydrogen addition effect onto the nox emission of an industrial combustor. Fuel 2022;328:125278.
[22] Nandula S, et al. Rayleigh/Raman/Lif measurements in a turbulent lean premixed combustor 34th Aerospace Sciences Meeting and Exhibit. 1996.
[23] Launder BE, Spalding DB. The numerical computation of turbulent flows. In: Numerical prediction of flow, heat transfer, turbulence and combustion. Pergamon; 1983. p. 96–116.
[24] Lewandowski MT, Płuszka P, Pozorski J. Influence of inlet boundary conditions in computations of turbulent jet flames. Int J Numer Methods Heat Fluid Flow 2018;28(6):1433–56.
[25] cd-adapco. STAR CCM+ version 11 User guide. Cd-adapco; 2016 [Online]. Available: https://stevedocs.cd-adapco.com/starccmplus_latest_en/index.html?param=eNUMK.
[26] Paul SC, Paul MC. Radiative heat transfer during turbulent combustion process. Int Commun Heat Mass Tran 2010;37(1):1–6.
[27] G.P. Smith, D.M. Golden, M. Frenklach, N.W. Moriarty, B. Eiteneer, M. Goldenberg, T. Bowman, R.K. Hanson, S. Song, W.C. Gardiner Jr., V.V. Lissianski, Z. Qin , [Online]. Available: http://www.me.berkeley.edu/gri_mech/.
[28] Van Oijen JA, Donini A, Bastiaans RJM, ten Thije Boonkkamp JHM, De Goey LPH. State-of-the-art in premixed combustion modeling using flamelet generated manifolds. Prog Energy Combust Sci 2016;57:30–74. 3.
[29] Department for Business, E.& I.S.. UK hydrogen strategy. GOV.UK; 2022. GOV.UK. Available at: https://www.gov.uk/government/publications/uk-hydrogen-strategy.